Self-regenerating compliance and lubrication of polyacrylamide hydrogels

Journal:	*Soft Matter*
Manuscript ID	SM-ART-08-2019-001607.R1
Article Type:	Paper
Date Submitted by the Author:	12-Sep-2019
Complete List of Authors:	Bonyadi, Shabnam; University of Illinois at Urbana-Champaign, Mechanical Science & Engineering Atten, Michael; University of Illinois at Urbana-Champaign, Mechanical Science & Engineering Dunn, Alison; University of Illinois at Urbana-Champaign, Mechanical Science & Engineering

SCHOLARONE™
Manuscripts

Self-regenerating compliance and lubrication of polyacrylamide hydrogels

Shabnam Z. Bonyadi[1], Michael Atten[1], Alison C. Dunn[1]*

[1]Department of Mechanical Science & Engineering, University of Illinois at Urbana-Champaign, Urbana, USA

*Corresponding Author:
Alison C. Dunn
MechSE @ UIUC
1206 W Green St MC 244
Urbana IL 61801
(217) 300-0349
acd@illinois.edu

1   ABSTRACT

2   Pristine hydrogel surfaces typically have low friction, which is controlled by composition,

3   slip speeds, and immediate slip history. The stiffness of such samples is typically measured

4   with bulk techniques, and is assumed to be homogeneous at the surface. While the surface

5   properties of homogeneous hydrogel samples are generally controlled by composition, the

6   surface also interfaces with the open bath, which distinguishes it from the bulk. In this

7   work, we disrupt as-molded polyacrylamide surfaces with abrasive wear and connect the

8   effects on the surface stiffness and lubrication to the wear events. At both the nanoscale

9   and the microscale, quasistatic indentations reveal a stiffer surface by up to two times

10   following wear events, even considering roughness. Longitudinal experiments with a series

11   of wear episodes interposed with periods of re-equilibration show that increased stiffness

12   is reversible: more compliant surfaces regenerate within 24 hours. The timescale suggests

13   an osmotic swelling mechanism, and we postulate that abrasive wear removes a swollen

14   surface layer, revealing the stiffer bulk. The newly-revealed bulk becomes the surface,

15   which re-swells over time. We quantify the effects on the self-lubricating ability of these

16   surfaces following abrasive wear using micro-tribometry. The lubrication curve shows that

17   robust low friction is maintained, and that the friction becomes less dependent upon the

18   sliding speed. The unique ability of these materials to regenerate swollen surfaces and

19   maintain robust low friction following abrasive wear is promising for designing their slip

20   behavior into aqueous soft robotics components or biomedicine applications.

21 1 INTRODUCTION

22 Slip systems in the body like the blink of the eye are created by tissues that have a layered

23 structure, wherein the outermost, softest layer holds water for excellent lubrication, and

24 deeper elements are able to support applied loads and withstand pressure [1,2]. The tear film

25 at the outermost surface maintains the balance of hydrated mucins, glycoproteins, and

26 lipids homeostatically through continual rejuvenation, which allows the eyelid to blink

27 down 10s of thousands of times per day without perceiving pain or fatigue [3,4]. The

28 branched, superhydrophilic nature of the mucins and glycoproteins holds water on the

29 surface of the eye between blinks, and the swelling of the entire network is limited by

30 entanglements and the network salt interactions [5,6]. In that way, the functionality of

31 maintaining hydration is determined by the combined mechanics of the fluid and polymer

32 components of the network [7–10].

33

34 Synthetic hydrogels, which differ from mucinous networks in their density and chemical

35 crosslinks, are being explored as biomimetic materials for sliding applications. They can

36 hold fluid with the aim of facilitating metabolism [11], and they are soft and slippery to

37 provide high-efficiency sliding [12–15]. Currently, synthetic hydrogels are being explored for

38 local repair or replacement of tissues like cartilage because of their remarkably low friction

39 coefficients and high compressive strength [16]. Work is also being done to improve other

40 mechanical properties of hydrogels including tensile strength [17], toughness [18], and

41 extensibility [19] by crosslinking two different polymers together to create double network

42 hydrogels.

43

44   Much work has been done tuning the properties of hydrogels to better match those of

45   cartilage, such as crosslinking, pore size, and addition of composites [20]. In order to leverage

46   load support and simultaneously provide low friction, surface layers have been

47   implemented by a variety of groups as well [21,22]. Whether neat or layered surfaces, these

48   hydrogels under frictional loading may be susceptible to weakening and wear. In hard

49   materials, efforts are beginning to be successful in connecting the friction and wear

50   behaviors by locating precisely where energy is dissipated within the surfaces [23], but with

51   soft materials the connections are not yet as clear.

52

53   The authors are aware of limited studies which attempt to quantify the wear behavior of

54   hydrogels.

55   In an effort to improve the wear resistance of hydrogels, groups have found that wear

56   decreases by decreasing hydrogel water content [24–26], increasing thickness [24], decreasing

57   preload [24], decreasing load [25,26], and increasing crosslink density [25,26]. However, studies

58   have found no relationship between friction coefficient and wear rate, which agrees with

59   the concept that friction and wear are two separate phenomena [25,26]. Accurately

60   quantifying the wear rate of hydrogels is an ongoing challenge because (1) hydrogels are

61   clear, environmentally sensitive materials and (2) the wear rate changes with the number

62   of wear cycles [24,27]. Because wear is defined as the removal of material from a surface, it is

63   intimately related to local failure phenomena. Flexible polymeric networks like elastomers

64   and hydrogels wear by the breaking of bonds under high strains, like the sacrificial wear of

65   a pencil eraser. However, for hydrogels, the breaking of bonds necessitates a local re-

66   equilibration of the network. It is this mechanism that can be locally induced by abrasive

67   wear, and which we aim to leverage in understanding the effects of abrasive wear to the

68   surface of a hydrogel, and specifically chemically-crosslinked polyacrylamide.

69

70   In this work, we systematically apply abrasive wear to the surface of polyacrylamide

71   hydrogels and assess the response of the surface over time using indentation both at the

72   nanoscale and at the microscale. We use the changes in surface stiffness trends found at

73   both scales to describe the time response of the surface following abrasive wear and

74   correlate the stiffness to local changes in surface composition through polymer physics

75   scaling laws. From the complementary results found at both scales, we postulate that

76   reduced-density surface layers are an inherent feature of water-equilibrated

77   polyacrylamide surfaces. We also assess the surface in micro-friction experiments and

78   discover that robust, low friction is maintained throughout repeated, longitudinal abrasive

79   wear. Finally, we estimate the rate of abrasive wear for fully-hydrated polyacrylamide.

80

81   2   MATERIALS AND METHODS

82   **2.1 Hydrogel Preparation.** Polyacrylamide hydrogel slabs were polymerized in standard 40

83   mm diameter polystyrene Petri dishes or polystyrene Petri dish lids for all experiments.

84   The height was limited to 1 mm for nanoscale tests and 5 mm for microscale tests. Molds

85   were capped with another polystyrene Petri dish such that buoyancy leveled the molded

86   surface. Simultaneous chain extension and crosslinking was done via a chemical initiator

87   and   radical   donor: 0.05%   ammonium   persulfate   (APS)   and   0.15%

88   tetramethylethylenediamine (TEMED). Pre-polymer solutions were 7.50% acrylamide,

89   0.39% bis-acrylamide, and 91.91% water, all on a mass per mass of total solution. This

90   composition was used because of its classification as an 'ideal network hydrogel' [20], as well

91   as empirical evidence that the swelling ratio does not change following synthesis (Q=1).

92   Samples were optically transparent, and no swelling was observed throughout all

93   experiments. Samples were stored at 4°C for more than 12 hours before experiments and

94   intermittently during longitudinal experiments to prevent bacterial growth. Samples were

95   handled with latex laboratory gloves, and allowed to equilibrate to room temperature

96   before starting experiments. Separate samples were created for nanoindentation and

97   microindentation due to the different setups of the two instruments.

98

99   **2.2 Nanoscale experiments**

100   *2.2.1 Experimental progression*

101   The general progression was to characterize pristine surfaces, apply controlled abrasive

102   wear, and immediately re-characterize the surfaces at ~25°C. Characterization consisted of

103   quasistatic indentation using atomic force microscopy (AFM); schematics of the technique

104   and experimental progression is shown in Figure 1, respectively. For longitudinal

105   experiments, this cycle was repeated two more times with periods of 72 hours of

106   submersion in water a 4°C for a total of three wear tests (n=3) on the same hydrogel

107   sample. The hydrogels were always submerged underwater during surface
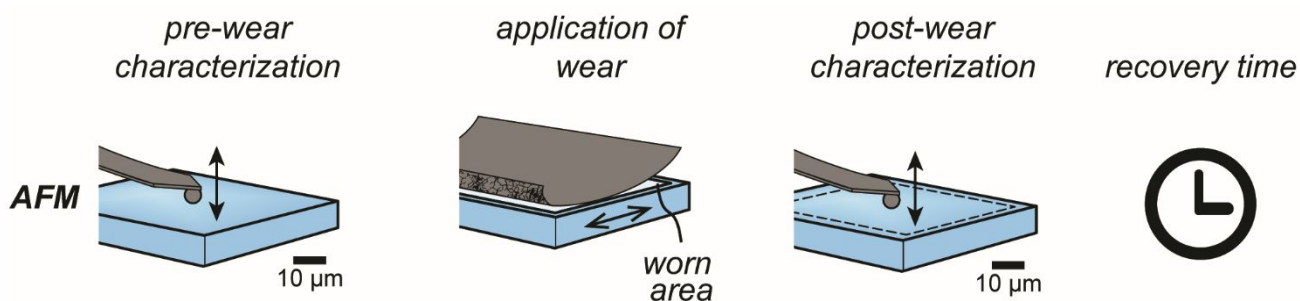
108   characterization and wear application to prevent the effects of dehydration in the results.

109   **Figure 1.** One experiment at the nanoscale follows this longitudinal progression. Indentation
110   was performed at the nanoscale using colloidal probe atomic force microscopy to characterize
111   the pre-wear surface. Afterwards, wear was applied across the entire surface of the hydrogel
112   using sandpaper. This was followed by another nanoindentation test to characterize the post-wear
113   surface. Samples were submerged underwater at ~25°C during surface characterization and wear
114   application. Finally, the samples were allowed to recover for times >24 hours at 4°C while still
115   submerged in water before the next experiment. For the nanoindentations, this experiment was
116   performed up to three times.

117   *2.2.2 Wear application*

118   Wear was applied using 1000 grit sandpaper with an average roughness (Ra) of 6.38 μm

119   and root mean square roughness (RMS) of 8.54 μm (Paxcoo Direct) to cause abrasive wear

120   to the hydrogel surface. The roughness values were obtained by scanning a 5.66 mm^2 area

121   of the sandpaper in a 3D Laser Scanning Confocal Microscope (Keyence VK-X1000). To

122   ensure that nanoindentations were performed on an area that was previously worn for our

123   longitudinal experiments, wear was applied across the entire hydrogel surface. The

124   samples were worn with sandpaper under a load that ranged 20-100 mN for 100 passes at

125   roughly 3 mm/s (lasting about 2 minutes). Throughout the duration of wear application,

126   the hydrogel was submerged underwater. Samples were rinsed to remove wear debris, re-

127   submerged under a fresh layer of water, and tested.

128

129   *2.2.3 Indentation*

130   Local stiffness measurements of the top few micrometers were achieved by quasistatic

131   nanoindentation through a 5 μm diameter colloidal glass probe (Bangs Labs, IN, USA), both

132   before and after applying wear. Standard silicon nitride cantilevers (stiffness $k = 0.1$ N/m,

133   NanoAndMore, CA, USA) indented at V_{indent}~23 μm/s in a 10x10 array spanning an area of 90

134   μm square (Figure 2) using the AFM (Asylum Research, model MFP-3D). This relatively low

135   stiffness was chosen to achieve measurable forces during small-depth indentations of the

136   sample [28]. In later experiments, colloidal probes were constructed by attaching a silica

137   microsphere (Bangs Labs, IN, USA) on a cantilever probe (NanoAndMore, CA, USA) using a

138   quick-dry epoxy (Bangs Labs, IN, USA). A diluted solution of colloids was dehydrated [29],

139   and an individual particle was placed on the probe tip using a micromanipulator [13].

140

141   The probe was calibrated in a standard fashion by measuring the inverse optical lever

142   sensitivity (InvOLS) by performing a force curve on a hard surface in air and again on a

143   hard surface in fluid. The stiffness (k = 0.1 N/m) was confirmed using the thermal method

144   [30]. The outside of the petri dish sample holder was glued to a glass microscope slide and

145   clamped down to the AFM stage to securely hold the hydrogel and prevent any motion

146   during the lateral movements of the probe.

147

148   To locate the surface before starting indentation, the probe was lowered until reaching the

149   pre-load. The probe was then raised out of contact with the surface to avoid embedding the

150   probe and to prevent sample interference during lateral motions between indents. Given

151   the roughness of the surface and the vertical clearance required, the probe displacement

152   during indents was set to its maximum value of 12 μm. While we collected the data for this

153   entire indentation range, we only analyzed the portion of the curve that was within the first

154   micron of indentation. Within this region, we found a 0.5 μm long portion that fit the Hertz

155   model to determine the surface modulus of elasticity. The confidence of the fitting and

156   fitted surface modulus of elasticity was increased through mapping of N=200 force curves

157   (two 10 x 10 maps at different locations) on each sample [31]. Force vs. indentation depth

158   data was collected on unworn hydrogel samples; the samples were then worn and rinsed to

159   remove wear debris. These worn samples underwent another series of indentations and

160   the data was analyzed in MATLAB.
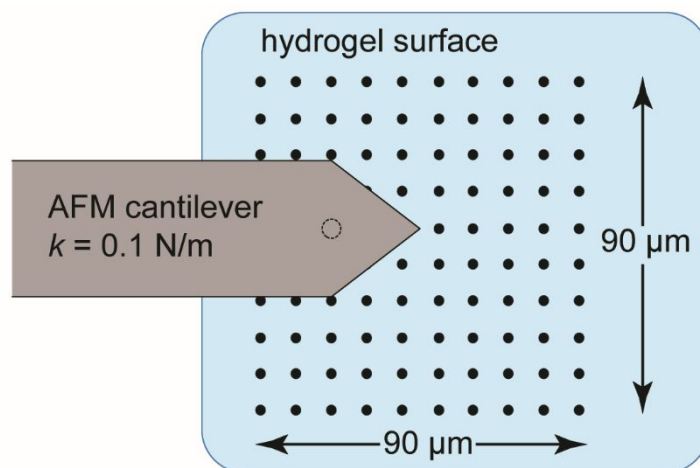
161   **Figure 2.** Schematic map showing the input locations for each of 100 quasistatic nanoindentation
162   measurements on the hydrogel surface over an area of 90 μm x 90 μm.

163   *2.2.4 Indentation analysis*

164   Indentation by an impermeable probe is well-suited for detecting changes in the

165   compliance of soft surfaces. Both nanoscale and microscale experiments were analyzed

166   similarly by fitting the force vs. indentation depth curves to a power law with exponent

167   *n*=1.5, i.e. the Hertz model. A discussion of the limits of this technique can be found

168   following the results. The fitting was done using a linear least-squares regression scheme

169   over a range of indentation depths for which the Hertz model applies, only up to a fraction

170   of the indenter radius. While small-strain theory states that the ratio of indentation depth

171   to probe radius needs to be less than or equal to 0.1 for the model to apply, recent work has

172   shown that this ratio is overly strict, particularly for soft materials with high Poisson ratios

173   ($v \geq 0.4$) [32,33]. In fact, Yoffe found that the Hertz model is valid (within 1% error) to

174   indentation depths at least up to 0.64*r*, where *r* is the radius of the probe. For our analysis

175   of the nanoindentations, we fit the Hertz model to a 0.5 μm long region of the curve within

176   the first micron of indentation, which is less than $0.64r$ (1.6 μm), where r is 2.5 μm. A

177   typical nanoindentation curve and corresponding fitting regime is shown in the bottom

178   graph of Figure 3. The modulus of elasticity as measured at the surface, which we denote as

179   the *surface modulus of elasticity*, is estimated using the Hertz model coefficient (Equation

180   1). This model requires the use of a Poisson ratio, which ranges from 0.3 to nearly 0.5 in

181   the literature, depending upon assumptions of the material character as an elastic solid

182   [34,35], viscoelastic solid [36], or poroelastic solid [37-39]. For the sake of consistency and ability to

183   compare results, ν=0.45 was used for all fits. Thus, the only free parameter was E, a

184   representative stiffness at the surface.

185    $$F = \frac{4}{3} R^{0.5} \frac{E}{1-\nu^2} d^{1.5}$$ (Equation 1)

186   In this work, we more specifically used a modification of the Hertz model, which eliminated

187   the need to know the point of contact [40]. By using the derivative of Equation 1 with respect

188   to displacement, the variable of indentation depth is removed. A plot of dF vs F that

189   illustrates the fitting method is shown in the top graph of Figure 3. We use the modulus

190   value derived from the top graph to draw the red Hertz line in the bottom graph. This

191   confirms that this innovative method of applying the Hertz model produces appropriate

192   stiffness values.
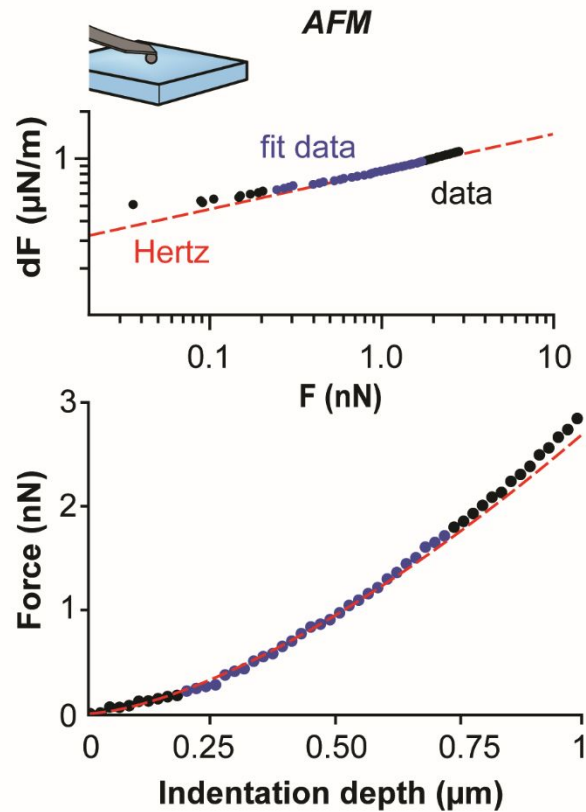
Figure 3. Quastistatic indentations at the nanoscale were fit over a 0.5 μm region using the derivative Hertz model to characterize the elastic response. The black circles are the raw data points and the blue circles indicate the data points used for fitting to the Hertz model. The top graph resembles those shown in the reference paper [40]. The bottom graph shows the portion of the curve used for analysis and how well the stiffness value obtained fits the curve, which is represented by the red-dashed line.

2.3 Microscale experiments

2.3.1 Experimental progression

Similar to the nanoscale experiments, the general experimental progression was to characterize pristine surfaces, apply controlled abrasive wear, and immediately re-characterize the surfaces at ~25°C. An instrumented microindenter with a lateral force transducer was used to characterize the surface through both microindentations and microfriction tests. Schematics of the experimental progression and characterization techniques are illustrated in Figure 4. For longitudinal experiments, this cycle was repeated five more times with periods of at least 48 hours of submersion in water a 4°C for a total of

208   six wear tests (n=6) on the same hydrogel sample. The results of additional hydrogels with

209   n=7 and n=3 wear tests are provided in the Supplementary Materials Figure S7. The
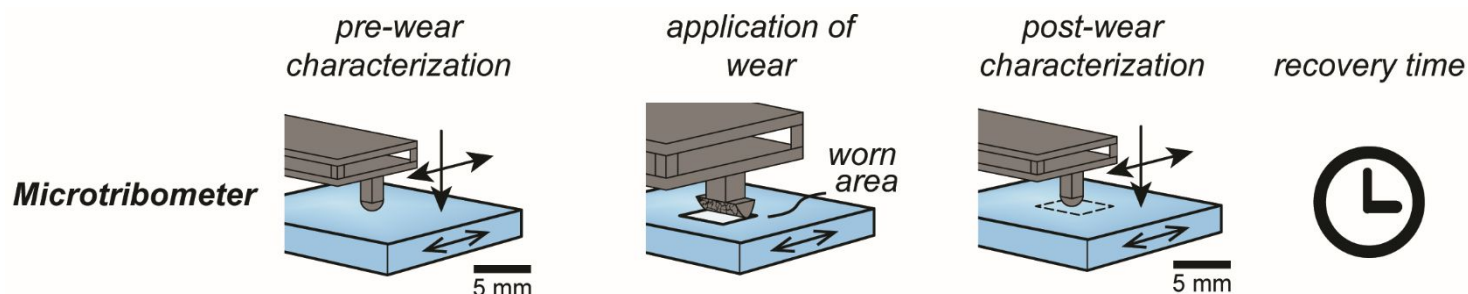
210   hydrogels were always submerged underwater during surface characterization and wear

211   application to prevent the effects of dehydration in the results.

212   **Figure 4.** Indentation and friction tests were performed at the microscale using a flexure-based
213   tribometer to characterize the pre-wear surface. Wear was applied using a semi-cylinder probe
214   covered with sandpaper and attached to the microtribometer that reciprocated under a defined set
215   of parameters. The probe was changed back to the steel ball to measure the post-wear stiffness
216   and friction. All characterization was done within the worn area, and repeated multiple times to
217   assess repeatability. During surface characterization and wear application, the samples were
218   submerged in a water bath at ~25°C. Finally, the samples were stored at 4°C for times >24 hours
219   while still submerged in water before the next experiment.

220   *2.3.2 Wear application*

221   For the microscale indentation and friction tests, a wear probe was fabricated from a semi-

222   cylinder with a radius of 3.75 mm and length of 3.5 mm covered in the sandpaper paper.

223   The probe reciprocated perpendicularly to its longitudinal axis at a load of 10 mN and

224   speed of 3,000 μm/s for 5,000 cycles (lasting about 2 hours); this load was selected due to

225   its ability to induce wear without extreme effects such as compression cracking, and the

226   speed was chosen for expediency of experiments without being so fast as to cause

227   dynamics effects. There was always a layer of water on the hydrogel while the probe wore

228   the surface. After wear application, hydrogels were rinsed to remove wear debris,

229   submerged under a fresh layer of water, tested, and returned to storage at 4°C. Because the

230   wear scar is not visible to the naked eye while the hydrogel is underwater, the elastic

231   repositioning method was implemented, in which multiple cavity engagements of the petri

232   dish and microtribometer stage ensured that wear was applied to the same location for

233   every test [41]. Wear was confined to an area of ~5.25 mm^2 in the center of the hydrogel

234   (Figure 4).

235

236   *2.3.3 Indentation*

237   Local stiffness measurements of the top 10s of micrometers were achieved by

238   microindentation through a 2 mm diameter spherical steel probe, both before and after

239   applying wear systematically using a custom swiping probe surfaced with 1000 grit

240   sandpaper. Custom four-bar cantilevers (stiffness $k = 538.83$ N/m) indented at V_{indent}~8-17

241   μm/s; while non-uniform rates, all indentation durations were far shorter than timescales of

242   poroelastic relaxation [37]. The normal load for all indentations was less than or equal to 1 mN.

243   The microtribometer measured the force with respect to indentation depth across a total of

244    $N=10$ indents on the same location.

245

246   *2.3.4 Indentation analysis*

247   The microindentations were analyzed using the same method as described for the
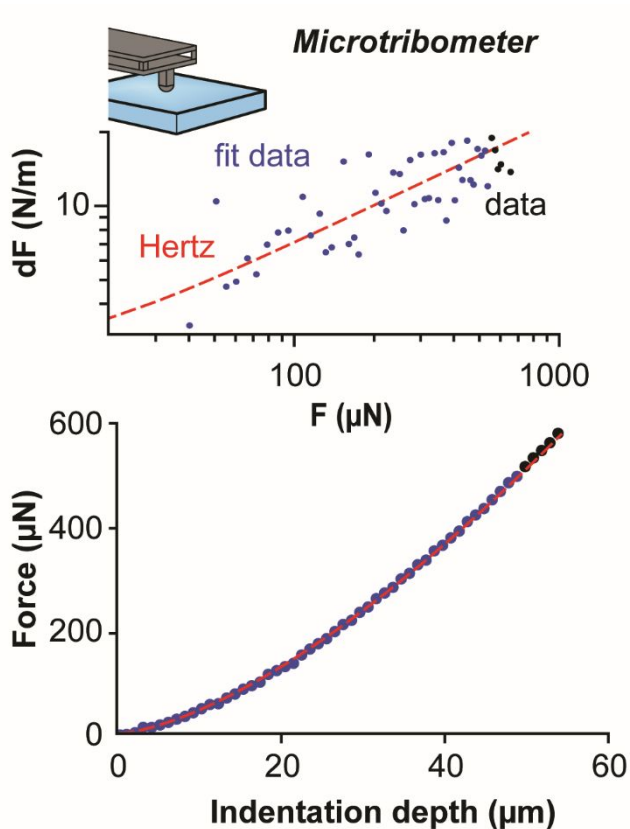
248   nanoindentations, in which the indentation curves were fit to a modified Hertz model. A

249   Poisson ratio of ν=0.45 was also used for fitting. For our analysis of the microindentations,

250   we fit a 50 μm region to the Hertz model, which is less than $0.64r$ (0.64 mm), where r is 1

251   mm; therefore, it fell within the small-strain range. A typical curve and fitting regime is

252   shown in Figure 5.

253   **Figure 5.** Quastistatic indentations at the microscale were fit over a 50 μm region using the
254   derivative Hertz model to characterize the elastic response. The black circles are the raw data
255   points and the blue circles indicate the data points used for fitting to the Hertz model. The top
256   graph resembles those shown in the reference paper [40]. The bottom graph shows the portion of
257   the curve used for analysis and how well the stiffness value obtained fits the curve, which is
258   represented by the red-dashed line.

259   *2.3.5 Friction*

260   Microscale friction measurements were done on the pre-wear and post-wear surfaces in

261   conjunction with the indentation experiments, using the same spherical steel probe. A

262   custom microtribometer that utilizes piezoelectric stages and milliscale flexures for motion

263   and load measurement performed these tests [42,43]. The probe applied a 1 mN force for a

264   stroke distance of 1.5 mm and speeds ranging from 500 μm/s to 4000 μm/s at increments

265   of 500 μm/s. The probe reciprocated 100 times for each speed and the coefficient of

266   friction was computed for each cycle using data from the middle 20% of the probe's path to

267   exclude effects from directional changes; typical data is shown in Figure 6. The

268   displacement of the probe was in the same direction as the wear application.
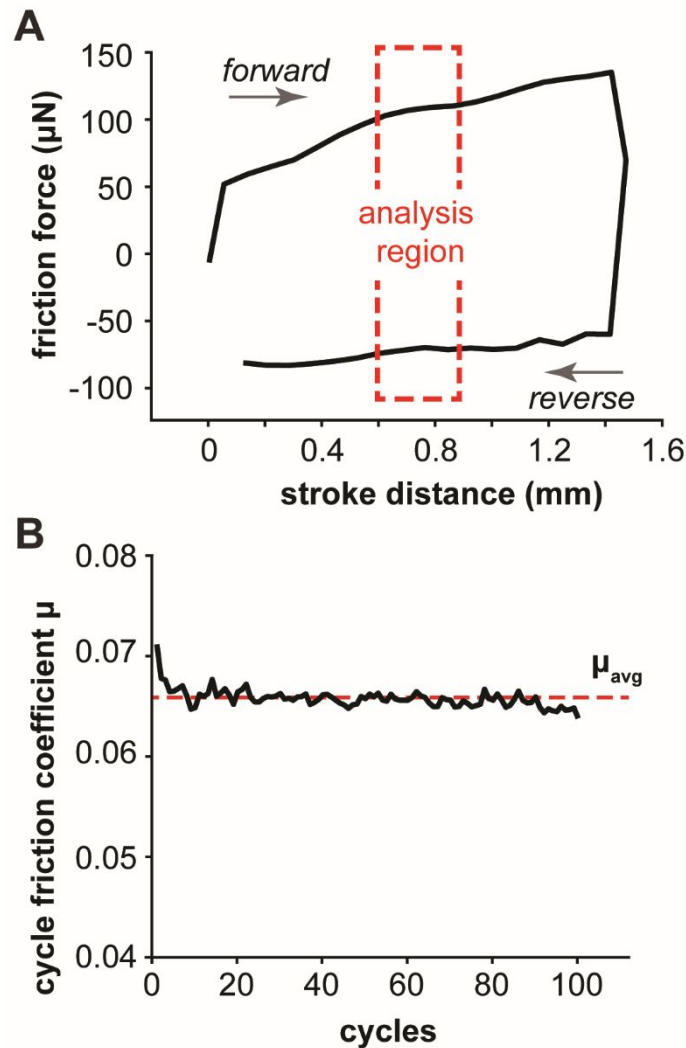
269   **Figure 6.** The progression of reporting the lubrication curve for pre-wear and post-wear samples.
270   (A) The hydrogel sample reciprocates underneath a 2 mm diameter spherical steel probe,
271   resulting in a friction force in forward and reverse directions. Only the boxed region is analyzed
272   to avoid speed effects at the reversals. The direction-averaged "cycle" friction coefficient is

273   calculated for each of the 100 cycles at a constant sliding speed. (B) After a brief run-in, the
274   friction coefficient converges to a steady-state value for that particular set of conditions; here the
275   representative value is μ_{avg}~0.066.

276   3   RESULTS AND DISCUSSION

277   **3.1 Wear effects on surface stiffness**

278   *3.1.1 Nanoscale indentation tests*

279   Maps of N=100 indentations on pristine samples showed low values of surface modulus,

280   with median typically $E_{PRE,med}$≈1.46 $\pm$ 0.31 kPa (Figure 7, top left). After 100 passes by the

281   abrasive paper, the median modulus increased to $E_{POST,Exp1}$=1.67 $\pm$ 0.26 kPa, an increase of

282   14% (Figure 7, top right). The significance of the increase in modulus due to wear was

283   confirmed through a two-sample t-test that had a p-value of $1.3 \cdot 10^{-7}$. Following 72 hours in

284   a water bath at 4°C, a second pre-wear surface modulus was measured to be $E_{PRE,Exp2}$≈1.30

285   $\pm$ 0.24 kPa; a similar stiffness to the pristine sample. The same wear experiment was

286   repeated twice more, and each time the surface modulus appeared to increase immediately

287   after wear. After re-equilibration in a water bath, the compliance of the surface recovered.

288   To emphasize the statistical significance, box-and-whisker plots of all N=200 results for

289   each condition are shown in Figure 8. The magnitude of the surface moduli is lower than

290   expected for a 7.5% w/w polyacrylamide hydrogel, but the repeatability of the

291   measurements and the effect of wear suggest that they are accurate. This is supported by

292   the finding that during synthesis of poly(N,N-dimethylacrylamide) hydrogels, a surface-

293   drive monomer compositional gradient develops, and the thickness of this gradient

294   depends on the properties of the mold [44]. The group found that the polymer density of the

295   surface in the first 500 nm of compression remains below the polymer density of the bulk.

296   For our AFM stiffness measurements, we analyzed the first 500 nm of indentation depth,

297   which explains the lower surface moduli values we found for the unworn hydrogels. Wear

298   removes this less dense layer, and exposes the higher polymer density bulk. Swelling

299   experiments on poly(N-isopropyl acrylamide) (PNIPAAm), showed that hydrogels with

300   varying polymer concentrations achieve equilibrium swelling ratios after about 24 hours

301   underwater [45]. Therefore, although the hydrogels are submerged underwater during wear,

302   they do not have enough time to re-equilibrate their surface before surface testing

303   immediately after wear; however, they do have enough time to achieve their desired

304   swelling ratio before the next set of experiments 3 days later.
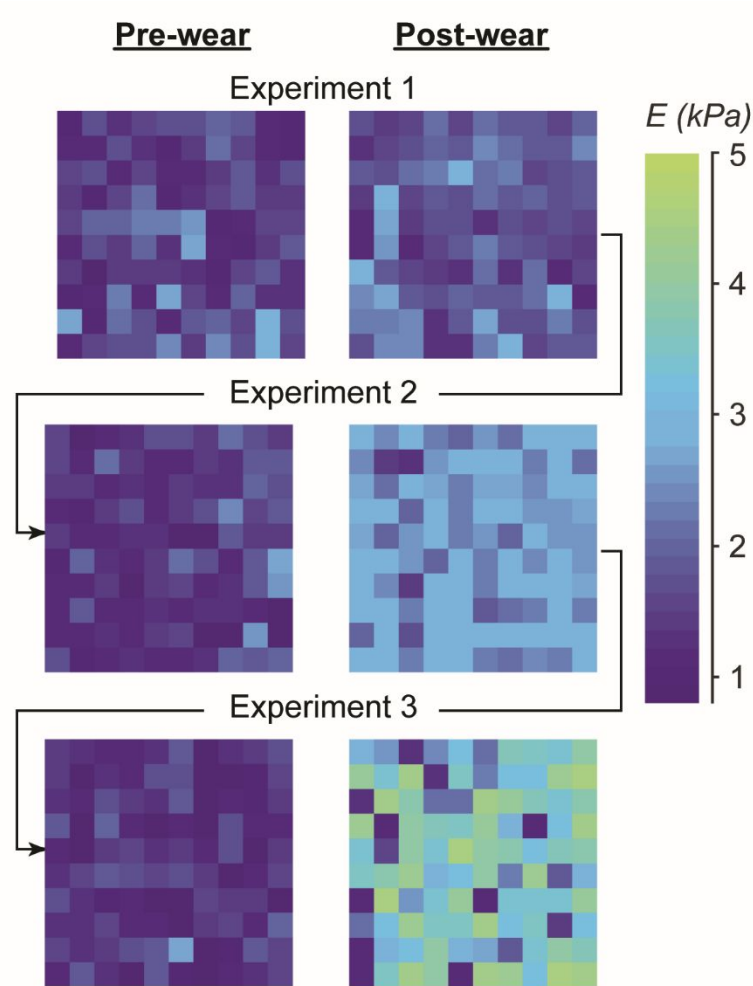
305   **Figure 7.** Contour maps showing the fitted surface modulus of elasticity distributions over the 90
306   μm x 90 μm area on a representative hydrogel surface as measured by quasistatic
307   nanoindentation. The wear was applied between pre-wear (left) contour maps and the post-wear

308   (right) maps. The arrows indicate the progression of $n=3$ serial experiments with ~72 hours
309   recovery time in between experiments. Generally, the average elastic modulus appeared to
310   increase immediately after the application of abrasive wear, shown by a lightening of the color
311   on the blue-green spectrum. As an example, the average and standard deviation of the surface
312   modulus for Experiment 3 was E_{PRE}=1.35 ± 0.35 kPa; it increased to E_{POST}=3.25 ± 0.98 kPa. The
313   magnitude of increase appeared to increase with subsequent experiments, and the range of values
314   also increased.
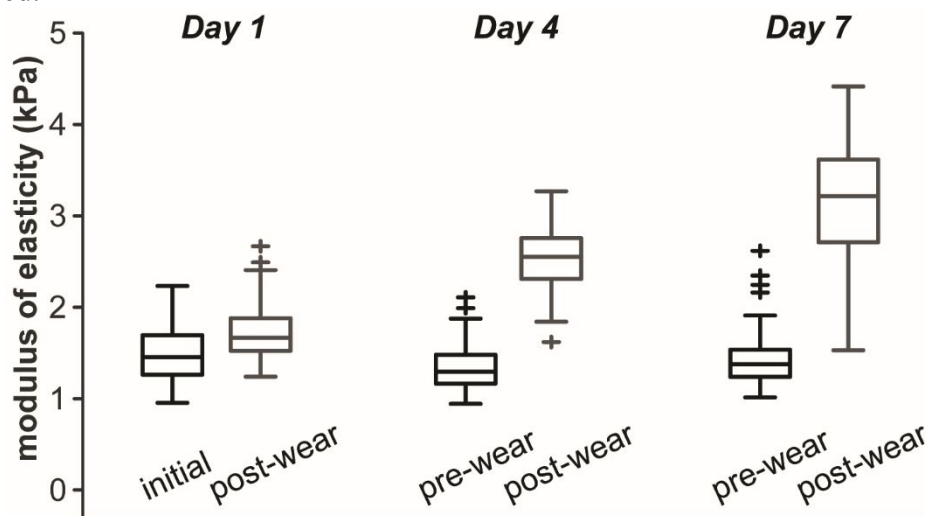
315   **Figure 8.** Box-and-whisker plots of the modulus of elasticity over longitudinal experiments at
316   the nanoscale. All measurements were identical. Each box and whisker plot represents 2 maps of
317   100 indentations each, in total N=200 at each condition. This quantifies the increased modulus
318   after wear, and the increasing variability in modulus after three experiments, performed over 7
319   days. After recovery in a water bath for 3 days, the elastic modulus recovered to the lower value
320   of E~1.4 kPa both times.

321   *3.1.2 Microscale indentation tests*

322   Microscale indentations complemented the information gained at the nanoscale by

323   leveraging a larger probe for ~24,400x larger contact areas while increasing the depth only

324   ~50x. At this scale a similar progression of stiffer post-wear surfaces was confirmed,

325   though with diminishing returns with subsequent wear experiments for $n=6$ repeated

326   cycles (Figure 9). Recovery time underwater returned these surfaces to a similar

327   compliance as that of an unworn hydrogel. As the experiment progressed, this recovery

328   was less pronounced, and the elastic modulus value on the recovered hydrogels never

329   reached the initial values seen on the unworn hydrogel. Over the span of 22 days, multiple

330   wear experiments were performed and the measured surface moduli were plotted. The
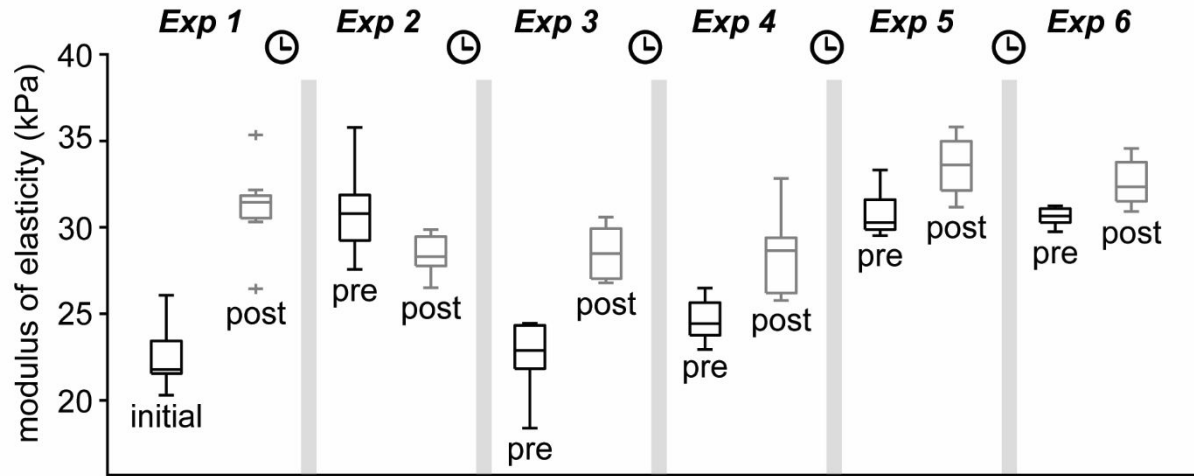
331   results confirmed the diminishing effect of wear, and that longer times to equilibrate

332   underwater, past 48 hours, did not result in more complete recovery (Figure 10). The

333   progression and the diminished degree of recovery suggest that up to $n=2$ or $n=3$ repeated

334   applications of abrasive wear, the surface retains some degree of uniformity. Subsequent

335   applications $n>3$ result in irrecoverable damage to the surface.

336   **Figure 9.** Box-and-whisker plots of the modulus of elasticity over multiple sets of longitudinal
337   experiments at the microscale. Each box and whisker plot represents the results of $N=10$
338   indentations on the same location of the hydrogel surface. We present one of three experimental
339   series in the manuscript, and provide the other two in the Supplementary Materials Figure S7.
340   The figure shows $n=6$ serial experiments, and the modulus of elasticity increased following wear
341   for 5 of the 6 experiments.

342   **Figure 10.** A linear time representation of the modulus changes measured at the microscale
343   shows that the values converge around 8 days into the series. The changes between pre-wear
344   measurements and post-wear measurements become confounded with subsequent experiments.
345   The time between wear experiments was a minimum of 48 hours (2 days), and day 0 corresponds

19
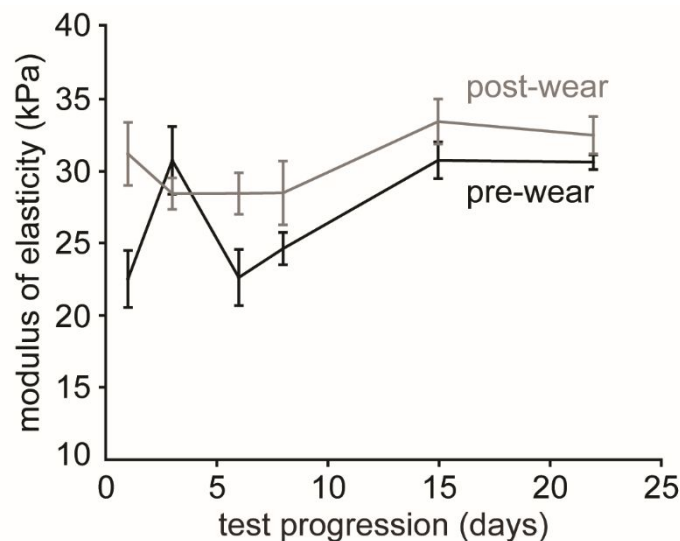
346   to the day in which the samples were polymerized. This figure shows the modulus of elasticity
347   evolution over the course of days.

348   *3.1.3 Interpretation of Stiffness Changes*

349   In general, the increased stiffness of the surfaces at both the nanoscale and microscale

350   immediately following wear events confirms a systematic effect. Although the nanoscale

351   and microscale are fundamentally different, we followed the most widely accepted

352   methods outlined in literature for indentation measurements at each scale, so the two

353   techniques proved to be complementary. Following wear, it is unlikely that the surface

354   remains compressed, or more dense, due to the migrating nature of the applied wear; there

355   is no constant applied pressure. This is confirmed by a study on the deformation of 7.5%

356   polyacrylamide hydrogels during local indentation tests and bulk compression tests [34]. The

357   researchers sequentially increased the load applied to the hydrogels in which each load is

358   held for 90 minutes and the amount of hydrogel compression is measured. They observed

359   no evidence of change in the thickness of the hydrogels for all loads below 10 kPa.

360   Considering that the osmotic pressure of 7.5% polyacrylamide hydrogels is about 11 kPa,

361   they concluded that hydrogels maintain Hertzian behavior at pressures below the osmotic

362   pressure of the hydrogel. By implementing the Hertz formula to describe the pressure at

363   the interface of cylinder on a flat plane (Equation 2), we calculated the highest pressure the

364   hydrogels experienced during our wear experiments. We applied a load (W) of 10 mN with

365   a probe that had a length (L) of 3.5 mm and radius (R) of 3.75 mm. To overestimate the

366   maximum pressure that occurs at the center of the contact (p_0), we used a reduced

367   modulus value (E^*) that is on the lower end. We calculated the highest pressure to be about

368   2.2 kPa, which confirms that hydrogels were not compressed.

369
$$p_0 = \left(\frac{W}{L} \frac{E^*}{\pi R} \right)^{1/2}$$
(Equation 2)

370   It is more likely, then, that a softer surface is worn away, revealing a stiffer bulk. This is

371   especially true because abrasive wear by sandpaper with a grit size of 1000 is expected to

372   leave the surface rougher – the resistance to compression by a number of asperities would

373   be lower than that of a flat elastic half space. The observed converse effect is thus further

374   confirmed.

375

376   The nanoscale and microscale stiffness measurements used to justify this effect of abrasive

377   wear should be considered here in the context of the applied pressures and local polymer

378   concentration of the surfaces. While the measurements at both scales show the same

379   general trend, the surface moduli from the fitting differ by a factor of 10, from a single

380   kilopascal at the nanoscale up to 10s of kilopascals at the microscale. In this work, we

381   compared the stiffness values at two depths/scales; however, to perform a thorough depth

382   dependent analysis of stiffness would require a greater range of probe sizes. Work on

383   polymers with different size and shape probes has been done, and the results showed that

384   the modulus values change based on the indentation depth [46]. Currently, the ranges and

385   sizes of probes do not allow for a continuous measurement at the nanoscale, microscale,

386   and milliscale, but such experiments have just been developed for hard materials [47], and in

387   the future may be used on soft surfaces.

388

389   At the nanoscale, the maximum indentation depth used for fitting was limited to $d<0.5$ μm

390   based on the colloidal probe radius of 2.5 μm. Assuming hemispherical exclusion, the

391   maximum interaction volume was 6.8 μm^3, and the average pressure at the maximum

392   applied load of 5.5 $\pm$ 2.2 nN was 0.70 $\pm$ 0.27 kPa. While this number appears low, it

393   reaches ~1/6th of the surface modulus at its stiffest, $E_{POST,Exp3}$=3.18 $\pm$ 0.61 kPa, and 1/3rd of

394   the surface modulus at its most compliant, $E_{PRE,Exp2}$=1.34 $\pm$ 0.24 kPa (see Figure 8). The

395   high pressure relative to the modulus suggests that the surface compliance is more

396   thoroughly interrogated on the local scale. Some of the surface roughness may cause

397   nonuniform contact against the colloidal probe, explaining the variability in the surface

398   modulus as shown in the modulus maps in Figure 7. However, because of the 200

399   indentations, only a few (typically 3 or fewer) outliers appear to engage the surface at an

400   unexpected location or display a nonphysical slope, the surface is flat enough to apply the

401   Hertz model. Furthermore, if the surface is not flat, and the colloidal probe vertically

402   approaches an angled surface the measured "normal force" will be reduced by the cosine of

403   the angle of tilt, and subsequent models would determine a more compliant surface than

404   reality. We find a stiffer surface, not a more compliant surface, following wear. If that is the

405   case, then our finding an increased surface stiffness is stronger confirmation of the effect.

406   We confirm that the spread of the box and whisker plots may represent the uncertainties of

407   the method itself to the values of modulus that we report, but when considering the source

408   of measurement uncertainty, the authors are unaware of more accurate techniques for

409   such a challenging surface.

410

411   At the microscale, correspondingly, the maximum indentation depth used for fitting was

412   limited to ~50 μm on the smooth steel sphere of radius 1 mm. The interaction volume was

413    $7.7 \cdot 10^6$ μm^3, and the average pressure at the maximum applied load of 583 $\pm$ 67 μN was

414   3.71 ± 0.43 kPa. In contrast to the nanoscale, this average pressure is only $1/22^{nd}$ of the

415   maximum surface modulus, and $1/14^{th}$ of the minimum surface modulus. This more

416   moderate pressure as compared to the surface modulus, along with the 24,400 times larger

417   contact area, corresponds to a more aggregate surface interrogation that is less affected by

418   surface changes in the top micrometers.

419

420   The character of the polyacrylamide surface was molded against polystyrene to be flat, but

421   the composition is likely to incur some gradient near the surface with the open bath at the

422   discontinuity where the swollen polymeric mesh meets the open bath. Sudre et al showed

423   using   neutron   reflectivity   measurements   and   shear   rheology   of   poly(N,N-

424   dimethylacrylamide) (PDMA) hydrogels that, "unless special precautions are taken, all gels

425   synthesized by simultaneous polymerization and cross-linking from the monomer will

426   have a surface-driven compositional gradient" [44]. In these studies of abrasive wear, we

427   leverage this lower density near the surface as the starting condition that is susceptible to

428   removal by abrasive wear. While the argument about mold material and fabrication

429   environment is helpful to explain that starting condition, it does not necessarily explain the

430   lower stiffness that is recovered when the worn surfaces are allowed to re-equilibrate

431   under an open water bath. While mold materials are important, we postulate that the

432   discontinuity between the osmotic balance of the swollen mesh and the negligible osmotic

433   environment of the open bath drives a local, polymer-diffusion-driven remodeling of the

434   surface over time. The hydrophilic network is inclined to swell because of the osmotic pull,

435   but the swelling is limited by the crosslinks and entanglements; breaking some of those

436   crosslinks and entanglements in the near surface will allow for very local swelling of the

437   surface. In our case, that long-time response of surface swelling and remodeling explains

438   the loss of stiffness in the newly-revealed polyacrylamide surfaces following abrasive wear.

439   Re-swelling of damaged hydrogels has only been previously observed in studies of

440   specialized hydrogels: one found that a fractured nanocomposite hydrogel surface was

441   initially stiffer than its undamaged counterpart, but the stiffness was lost over time [48]; the

442   other found lower stiffness of double network hydrogels at some time following fracture [49].

443   These studies hypothesized that the damaged network of the hydrogels leads to excess

444   expansion during swelling, though they did not apply the concept more generally.

445   Additionally, we had performed the same series of experiments on hydrogels with a

446   smooth steel ball probe as the wear applicator instead of a cylindrical sandpaper probe. We

447   have included the results of these experiments in the Supplementary Materials (Figure S1,

448   S2, S3) to emphasize the very small thickness of the surface of the hydrogels that dictates

449   its stiffness and friction behavior. The hydrogels from these experiments had lower wear

450   volumes; however, the results of the mechanical tests resembled that of the sandpaper

451   probe experiments detailed in this manuscript. These experiments further confirm that

452   hydrogel wear with high loads causes bond breakage and deformations to the surface

453   network architecture [50]. And because single network hydrogels have low toughness, with

454   only small strains, cascades of micro-fractures can occur [51]. To confirm that wear removes

455   a soft, surface layer to reveal a stiffer bulk, we performed experiments comparing the

456   surface and bulk moduli of hydrogels and included the results of these experiments in the

457   Supplementary Materials Figures S4-S5. After allowing the hydrogels to polymerize in a

458   water bath for >24 hours, we measured the surface stiffness. Within 10 minutes, we cut the

459   hydrogel in half, and measured the stiffness of the "bulk" surfaces. We found that the bulk

460   of the hydrogel is stiffer than the surface.

461

462   Horkay and Lin discuss the solvent/polymer relationship in polyvinyl alcohol (PVA)

463   hydrogels as a diffusion-driven process, which under varying solvent conditions must

464   contend with heterogeneous domains. Their conclusion is that the elastic modulus of

465   swollen gels is determined by the overall polymer concentration [52]. In this work, we can

466   use their universal scaling to calculate the drop in polymer concentration due to re-

467   equilibration of an abraded surface in the water bath (Equation 3); the storage modulus G

468   has been replaced by the surface elastic modulus E, φ represents the polymer volume

469   concentration, and the subscript e indicates those quantities in water equilibrium before

470   wear.

471
$$\frac{E}{E_e} = \left(\frac{\varphi}{\varphi_e}\right)^{0.42} \qquad \text{(Equation 3)}$$

472   Because the ratio of the storage modulus at a given state versus its equilibrium state is

473   analogous to the ratio of the Young's modulus at a given state versus its equilibrium state,

474   this equation is used as a pseudo-quantitative descriptor of the decreased density near the

475   surface due to the wear. The most appropriate stiffness value for the reference state is the

476   highest modulus measured after the abrasion, as it best represents the bulk stiffness. For

477   the nanoscale experiments this is $E_{POST,Exp3}$=3.18 ± 0.61 kPa, and the polymer concentration

478   is ~8%. From that reference state, the re-equilibrated surface with a modulus of

479     $E_{PRE,Exp2}$=1.34 ± 0.24 kPa has a polymer concentration of 1.0%, or ~8x drop in

480   concentration. The corresponding calculation for the microscale experiments using a

481   reference modulus of 36 kPa shows concentration decreases of only 2x, which makes sense

482   because deeper indentations should have stiffness that is closer to the bulk. Figure 11B

483   provides a reference for the indentation depths of the two scales; the nanoscale indents

484   travel primarily within the softer surface gradient whereas the microscale indents travel

485   through the entire surface gradient and into the bulk. Therefore, it is expected that the

486   nanoscale indents would show a greater change in stiffness due to wear; however, it has

487   been shown that softer surface layers influence the measurements of indentations into the

488   bulk [22], which is why the microscale also shows a change in stiffness due to wear. Although

489   the numbers derived using Equation 3 are the consequence of a model estimation, the

490   trends of these values confirm our description of the morphology of the hydrogel surface

491   after wear.

492

493   Overall, from these measurements, it is clear that surface compliance is recovered

494   following abrasive wear, and the surfaces spontaneously "regenerate" their surface

495   character during re-equilibration in a fluid bath (Figure 11A). This property is likely unique

496   to dilute swollen network hydrogels like polyacrylamide due to their hydrophilic nature

497   and osmotic pressure in the range of the applied pressure [34].
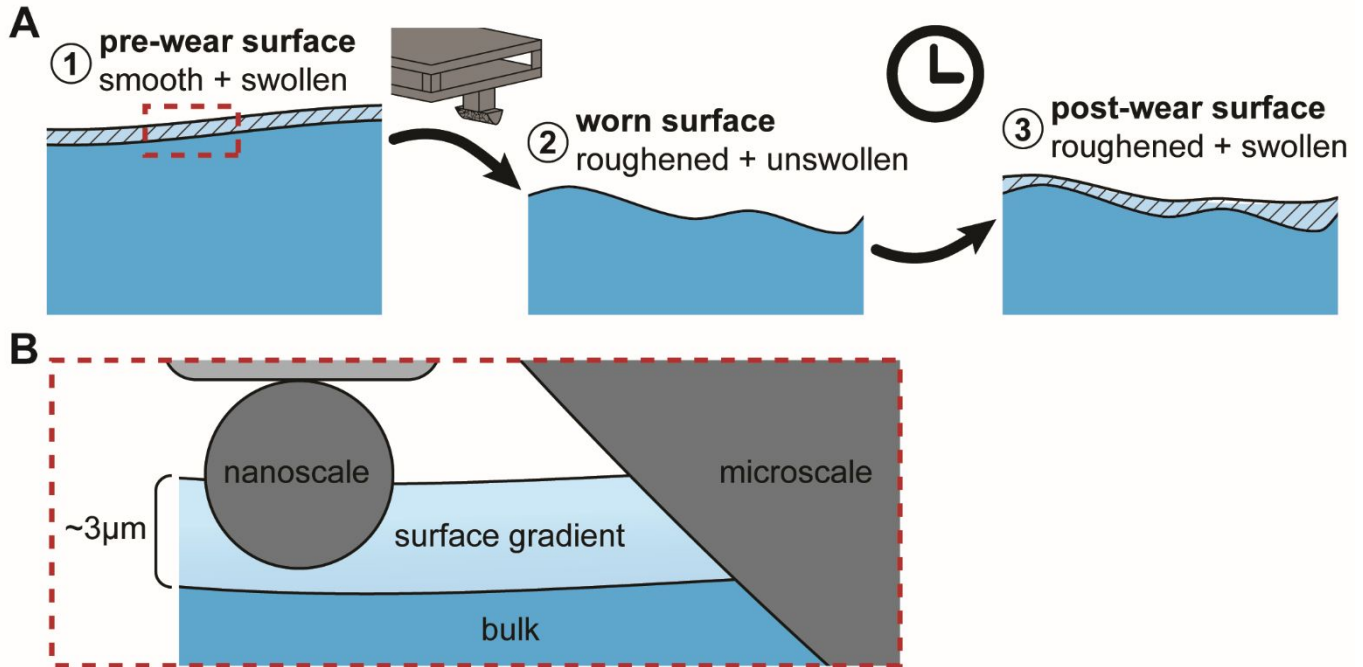
Figure 11. (A) Polyacrylamide surfaces undergo time-dependent surface regeneration following abrasive wear. In the pre-worn state (1), they are as smooth as the mold in which they were fabricated and appear to be very compliant at the surface, as in a very thin swollen layer as shown by Sudre et al [44]. In the just-worn state (2), the surfaces are rougher, but also increase in stiffness; this suggests that a softer layer was worn away. After long times stored in a submerged water bath (3), the surface compliance was recovered, indicating that the surfaces re-swell and regenerate favorable properties. (B) True to scale close-up of the region enclosed by the red-dashed box of the pre-wear surface with the two different sized probes. Only a part of the microscale probe is shown in the schematic because the microscale probe (r=1 mm) had a radius 400 times greater than that of the nanoscale (r=2.5 μm). The Hertz fits for the nanoscale and microscale indentations captured the top 0.5 μm and 50 μm of the surface, respectively. Therefore, nanoindentation measurements of the pre-wear surfaces remained within the surface gradient region while a greater portion of the microindentations were in the bulk. By removing this surface gradient layer through wear, it is expected that the nanoindentations would show a greater percent change in stiffness due to wear than the microindentations, which our results confirm.

3.2 Wear effects on lubrication

A surface property of hydrogels often leveraged is their lubricity, or low friction. For traditional engineering materials, wear-induced roughness or entrained third bodies can lead to higher friction and a loss of system efficiency. The original hypothesis that the surface would appear to be more "torn up" following abrasion was expected to lead to higher friction as a more compliant surface increased the contact area. The average friction

520   coefficients between the steel sphere and the polyacrylamide surfaces over eight speeds

521   (500-4000 μm/s in 500 μm/s increments) were analyzed together as lubrication curves,

522   presented in Figure 12A. The relationship between friction coefficient and slip speed in

523   traditional oil/metal contacts indicates the extent to which the viscous drag of the lubricant

524   contributes to friction [53]. In this case since the specific mechanisms driving hydrogel

525   lubrication are still not completely understood [12,38,54–57], we take the changes in the power

526   law exponent, α, of the friction versus slip speed to indicate the robustness of the

527   lubrication performance before and after wear events (Equation 4). The rate of rise of the

528   curves immediately following wear is lower than that after equilibration, indicating that

529   friction of the worn surfaces has a lower dependence on speed. However, similar to the

530   stiffness response, the time spent re-equilibrating in the water bath allowed the hydrogels

531   to recover their speed-dependent properties: the subsequent pre-wear curves have steeper

532   slopes than their post-wear counterparts.

533
$$\left(\frac{\mu}{\mu_0} \right) \propto V^{\alpha} \qquad\qquad \text{(Equation 4)}$$

534

535   In Equation 4, V is the velocity, μ is the friction coefficient at that velocity, and μ_0 is the
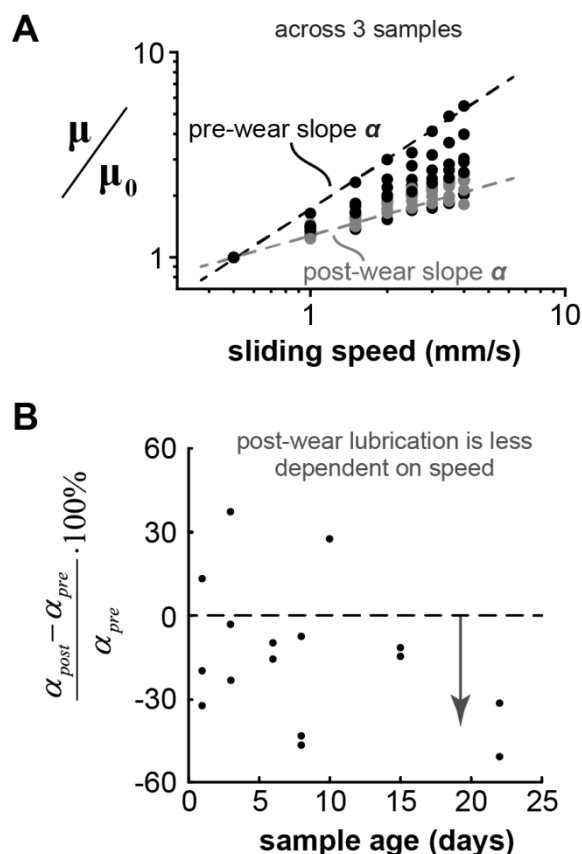
536   friction coefficient at the lowest speed for each curve (normalizing value for each series).

537   **Figure 12.** (A) Friction measurements were conducted at eight different speeds between V=0.5
538   mm/s and V=4 mm/s, and the results are plotted as a lubrication curve of normalized friction
539   coefficient versus sliding speed. A power law relationship with exponent α was used to quantify
540   the relative increase in friction with sliding speed; in general, the friction is more sensitive to
541   sliding speed before it is worn. (B) The percent decrease of α between the pre-wear and post-
542   wear state of each sample was calculated to quantify the effect of wear on the lubrication curves.
543   In the majority of experiments, wear caused the sample's friction performance to be less
544   sensitive to sliding speed. The time between wear experiments was a minimum of 48 hours (2
545   days), and day 0 corresponds to the day in which the samples were polymerized. This figure
546   shows the degree of slope change over the course of days.

547   In order to explicitly connect the pre-wear and post-wear measurements for each

548   experiment, the change in α was analyzed as a percent change due to wear and, more

549   specifically, as a percent decrease. Over all wear experiments (N=16), the majority had a

550   decrease in α, shown in Figure

551   12B, which means the frictional response tended to be less dependent on slip speed

552   immediately after wear. Soft surface layers with lower polymer density than the bulk have

553   shown to exhibit robust low friction due to the load support of the bulk and the lubricity of

554   the surface layer [22,58]; our results also show this. While those studies describe surface

555   layers of 3 μm thickness or greater, the surface layers in this study are expected to be equal

556   or thinner; this is based on the roughness of the sandpaper used to create the abrasive

557   wear and the inability to detect vertical swelling following abrasion.

558

559   While we saw a change in slope of the lubrication curves after wear, the friction coefficient

560   values remained within the same range of 0.02 to 0.05. Graphs of the raw (not normalized)

561   friction data can be seen in the Supplementary Materials Figure S8. This indicates that

562   surface wear does not compromise the effective lubricity of polyacrylamide hydrogels.

563   When considering the complexity of synovial fluid and the surface molecules of cartilage,

564   surface wear would remove these critical molecules and could have significant

565   consequences on the lubrication within joints. In the search for the underlying cause of the

566   less efficient lubrication mechanism of osteoarthritic cartilage, Klein and colleagues have

567   been investigating hydration lubrication, in which hydrated ions are trapped between

568   charged surfaces [59]. Evidence shows that these hydration shells contribute to the incredibly

569   low (μ~0.001) friction coefficients observed in joints. By trapping hydrated ions between

570   surfaces [60], coating surfaces with hydrated polymer brushes [61], and attaching hyaluronic

571   acid with phosphatidylcholines [62], they worked to better understand the lubrication of

572   cartilage surfaces. Hydrogels resemble the collagen network that holds the essential

573   lubricating molecules on the surface of cartilage. The work in this paper is one step

574   towards understanding the wear behavior of the collagen network. As groups continue to

575   isolate different components of cartilage, the breakdown of efficient lubrication of

576   osteoarthritic cartilage will be better understood.

577

578   **3.3 Surface Morphology**

579   In this work, we have so far detailed effects on the local composition and lubrication

580   performance of a polyacrylamide surface following a series of abrasion and recovery

581   experiments. Those results are generally encouraging for slip surfaces which may be used

582   against external or internal physiological tissues: soft surface character recovers, and

583   robust low friction is maintained. However, the traditional definition of *wear* is the gradual

584   removal of material, and particulates released from the surface may be less desirable. As a

585   final aspect of this work, we confirm the removal of material due to the abrasion and

586   estimate the wear rate of polyacrylamide under moderate abrasion.

587

588   After wearing the surface of the hydrogels, we did not observe wear particulates due to the

589   transparency of the hydrogel. However, when we completed the entire series of

590   longitudinal experiments on the hydrogels tested with the microtribometer, we removed

591   the layer of water to better observe the surface. We clearly identified an area ($\sim$2 mm x 4

592   mm) in the middle of the hydrogel that was visibly scratched into the surface, which we

593   have included in our Supplementary Materials Figure S6. To complement the mechanical

594   tests done in this work, we confirm the removal of material due to the abrasion and

595   estimate the wear rate of polyacrylamide under moderate abrasion.

596

597   Upon completion of the last wear test (7th wear test) of the longitudinal series on a single

598   hydrogel worn with the microtribometer for a total of 35,000 cycles, the worn surface was

599   imaged using a confocal microscope (Nikon) to estimate the volume loss (Figure 13). To

600   reveal the surface of the transparent sample, a solution of 1% solid yellow-green

601   fluorescent microbeads with 1 μm diameter and excitation/emission values of 505 nm/515

602   nm (ThermoFisher Scientific) was deposited on the surface. After sufficient time for the

603   beads to settle among the peaks and valleys of the roughened surface (~1 hour), a stack of

604   images was captured using a 10x objective. The vertical stack height was 200 μm with

605   spacing every 2 μm. From two adjacent volumes spanning the unworn and worn regions,

606   the wear depth following 7 wear tests was measured to be ~60 μm (Figure 14). The wear

607   volume was calculated within the region imaged, which is the product of wear depth (60

608   μm) and the image area (771 μm x 771 μm). From this, the volume was 0.0357 mm^3. One

609   simple way to quantify the progression of wear is through the Archard wear rate k, defined

610   as the wear volume normalized by the applied normal load and the slip distance [53]

611   (Equation 5). Because the wear volume measured only represents the volume loss in the

612   image area, we used the stroke length of 771 μm to obtain a total sliding distance of 54

613   meters (35,000 cycles x 771 μm x 2). Using the slip distance over the surface area in the

614   volume of interest (d=54 m) and the applied load of 10 mN, the wear rate is k= 6.6·10^{-2}

615   mm^3/(N·m). This wear rate should be considered approximate due to the optical distortion

616   of the spherical beads used as markers which likely blurred more than expected due to the

617   very rough surface scattering light. Even so, this wear rate falls near the same order as

618   unfilled polytetrafluoroethylene (PTFE) [63]. This indicates that though our application of

619 wear was rather severe because of the sharp abrasive particles of the sandpaper, the dilute

620 polyacrylamide resisted surface damage to a similar extent as unfilled PTFE that was worn

621 with a polished steel countersurface. This preliminary calculation of the Archard wear rate

622 is encouraging based on recent developments in super-tough double network hydrogels

623 [64,65], which one would expect to better resist wear.

624 $$k = \frac{V}{F_N d}$$ (Equation 5)
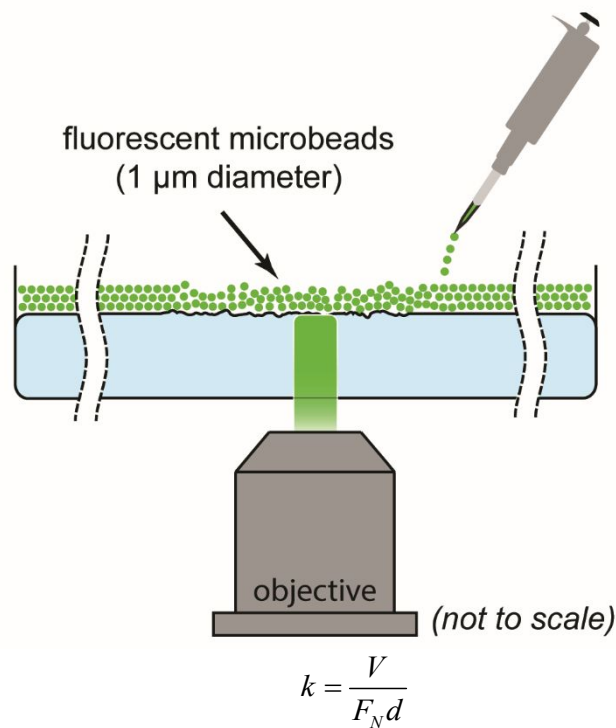
625 **YYFigure 13.** Hydrogel surface imaging technique using fluorescent microbeads and confocal
626 fluorescence microscope. Fluorescent microbeads in a solution were added to the surface of the
627 hydrogel. Images were taken once the beads had enough time to settle on the surface (~1 hour).
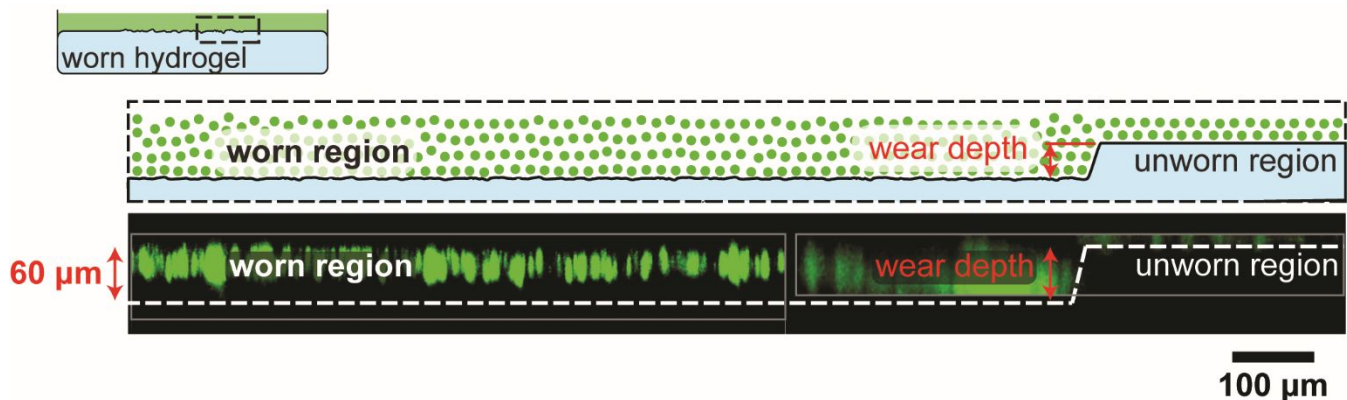
628 **Figure 14.** Microscopy confirmed that the samples experienced wear. A solution of 1 µm
629 fluorescent polystyrene beads was used to reveal the surface heights and estimate the wear depth.
630 The top two figures are schematics that elucidate the bottom figure, which is the image we
631 captured from the microscope. Two adjacent image stacks are shown as the maximum intensity
632 projection from the side, effectively a cross-section through an edge of the wear scar, traced in
633 the white dashed line. In this case the wear scar was quite deep, reaching up to $d{\sim}60$ µm.

634

635 4   CONCLUSION

636 Abrasive wear has measurable effects on hydrogel surface stiffness and lubrication. It

637 increases surface stiffness, widens the distribution of elastic modulus values, and decreases

638 the hydrogel frictional dependence on speed. Confocal imaging revealed thinning of the

639 hydrogel, offering a visual confirmation of the effects abrasive wear. The abrasive wear

640 removed a soft swollen surface layer to reveal the stiffer bulk; however, the bulk appears to

641 re-swell into the character of the pre-worn surface: more compliant and with the

642 corresponding higher dependence of friction on sliding speed. These results demonstrate

643 that hydrogel surfaces are self-regenerating. These conclusions have implications for the

644 use of hydrogels in load-bearing applications in the human body with unknown wear

645 behavior. This work raises questions about the effects of wear on other soft synthetic and

646 biological swollen networks.

647

REFERENCES

(1)   Pitenis, A. A.; Urueña, J. M.; Hormel, T. T.; Bhattacharjee, T.; Niemi, S. R.; Marshall, S. L.; Hart, S. M.; Schulze, K. D.; Angelini, T. E.; Sawyer, W. G. Corneal Cell Friction: Survival, Lubricity, Tear Films, and Mucin Production over Extended Duration in Vitro Studies. *Biotribology* **2017**, *11*, 77–83.

(2)   Braun, R. J. Dynamics of the Tear Film. *Annu. Rev. Fluid Mech.* **2012**, *44* (1), 267–297.

(3)   Dartt, D. A. *Regulation of Mucin and Fluid Secretion by Conjunctival Epithelial Cells*; 2002; Vol. 21, pp 555–576.

(4)   Rolando, M.; Zierhut, M. The Ocular Surface and Tear Film and Their Dysfunction in Dry Eye Disease. *Surv. Ophthalmol.* **2001**, *45 Suppl 2* (March), S203–S210.

(5)   Chen, H. B.; Yamabayashi, S.; Ou, B.; Tanaka, Y.; Ohno, S.; Tsukahara, S. Structure and Composition of Rat Precorneal Tear Film: A Study by an in Vivo Cryofixation. *Investig. Ophthalmol. Vis. Sci.* **1997**, *38* (2), 381–387.

(6)   Wagner, C. E.; Turner, B. S.; Rubinstein, M.; McKinley, G. H.; Ribbeck, K. A Rheological Study of the Association and Dynamics of MUC5AC Gels. *Biomacromolecules* **2017**, *18* (11), 3654–3664.

(7)   Trabbic-Carlson, K.; Setton, L. A.; Chilkoti, A. Swelling and Mechanical Behaviors of Chemically Cross-Linked Hydrogels of Elastin-like Polypeptides. *Biomacromolecules* **2003**, *4* (3), 572–580.

(8)   Kim, D.; Park, K. Swelling and Mechanical Properties of Superporous Hydrogels of Poly(Acrylamide-Co-Acrylic Acid)/Polyethylenimine Interpenetrating Polymer Networks. *Polymer (Guildf).* **2004**, *45* (1), 189–196.

(9)   Chang, D. P.; Abu-Lail, N. I.; Guilak, F.; Jay, G. D.; Zauscher, S. Conformational Mechanics, Adsorption, and Normal Force Interactions of Lubricin and Hyaluronic Acid on Model Surfaces. *Langmuir* **2008**, *24* (4), 1183–1193.

(10)   Weigand, W. J.; Messmore, A.; Tu, J.; Morales-Sanz, A.; Blair, D. L.; Deheyn, D. D.; Urbach, J. S.; Robertson-Anderson, R. M. Active Microrheology Determines Scaledependent Material Properties of Chaetopterus Mucus. *PLoS One* **2017**, *12* (5), 1–19.

(11)   Billings, N.; Birjiniuk, A.; Samad, T. S.; Doyle, P. S.; Ribbeck, K. Material Properties of Biofilms—a Review of Methods for Understanding Permeability and Mechanics. *Reports Prog. Phys.* **2015**, *78* (3).

(12)   Gong, J. P. Friction and Lubrication of Hydrogels - Its Richness and Complexity. *Soft Matter* **2006**, *2* (7), 544–552.

(13)   Shoaib, T.; Heintz, J.; Lopez-Berganza, J. A.; Muro-Barrios, R.; Egner, S. A.; Espinosa-Marzal, R. M. Stick-Slip Friction Reveals Hydrogel Lubrication Mechanisms. *Langmuir* **2018**, *34* (3), 756–765.

(14)   Urueña, J. M.; McGhee, E. O.; Angelini, T. E.; Dowson, D.; Sawyer, W. G.; Pitenis, A. A. Normal Load Scaling of Friction in Gemini Hydrogels. *Biotribology* **2018**, *13* (January), 30–35.

(15)   Lee, S.; Spencer, N. D. Sweet, Hairy, Soft, and Slippery. *Science (80-.).* **2008**, *319*, 575–576.

(16)   Gong, J. P.; Katsuyama, Y.; Kurokawa, T.; Osada, Y. Double-Network Hydrogels with Extremely High Mechanical Strength. *Adv. Mater.* **2003**, *15* (14), 1155–1158.

(17)   Zhu, L.; Xiong, C.; Tang, X.; Wang, L.; Peng, K.; Yang, H. A Double Network Hydrogel with High Mechanical Strength and Shape Memory Properties. *Chinese J. Chem. Phys.*

2018, *31* (3), 350–358.

(18) Na, Y. H. Double Network Hydrogels with Extremely High Toughness and Their Applications. *Korea Aust. Rheol. J.* 2013, *25* (4), 185–196.

(19) Engle, K. M.; Mei, T-S.; Wasa, M.; Yu, J.-Q. Highly Stretchable and Tough Hydrogels. *Acc. Chem. Res.* 2008, *45* (6), 788–802.

(20) Denisin, A. K.; Pruitt, B. L. Tuning the Range of Polyacrylamide Gel Stiffness for Mechanobiology Applications. *ACS Appl. Mater. Interfaces* 2016, *8* (34), 21893–21902.

(21) Blum, M. M.; Ovaert, T. C. A Novel Polyvinyl Alcohol Hydrogel Functionalized with Organic Boundary Lubricant for Use as Low-Friction Cartilage Substitute: Synthesis, Physical/Chemical, Mechanical, and Friction Characterization. *J. Biomed. Mater. Res. - Part B Appl. Biomater.* 2012, *100 B* (7), 1755–1763.

(22) Dunn, A. C.; Urueña, J. M.; Huo, Y.; Perry, S. S.; Angelini, T. E.; Sawyer, W. G. Lubricity of Surface Hydrogel Layers. *Tribol. Lett.* 2013, *49* (2), 371–378.

(23) Argibay, N.; Chandross, M.; Cheng, S.; Michael, J. R. Linking Microstructural Evolution and Macro-Scale Friction Behavior in Metals. *J. Mater. Sci.* 2017, *52* (5), 2780–2799.

(24) Suciu, A. N.; Iwatsubo, T.; Matsuda, M.; Nishino, T. A Study upon Durability of the Artificial Knee Joint with PVA Hydrogel Cartilage. *JSME Int. J. Ser. C* 2004, *47* (1), 199–208.

(25) Freeman, M. E.; Furey, M. J.; Love, B. J.; Hampton, J. M. Friction, Wear, and Lubrication of Hydrogels as Synthetic Articular Cartilage. *Wear* 2000, *241* (2), 129–135.

(26) Katta, J. K.; Marcolongo, M.; Lowman, A.; Mansmann, K. A. Friction and Wear Behavior of Poly(Vinyl Alcohol)/Poly(Vinyl Pyrrolidone) Hydrogels for Articular Cartilage Replacement. *J. Biomed. Mater. Res. Part A* 2007, *83A* (2), 471–479.

(27) Kim, C. L.; Kim, D. E. Durability and Self-Healing Effects of Hydrogel Coatings with Respect to Contact Condition. *Sci. Rep.* 2017, *7* (1), 1–11.

(28) Nalam, P. C.; Gosvami, N. N.; Caporizzo, M. A.; Composto, R. J.; Carpick, R. W. Nano-Rheology of Hydrogels Using Direct Drive Force Modulation Atomic Force Microscopy. *Soft Matter* 2015, *11* (41), 8165–8178.

(29) Bangs Laboratories. Product Data Sheet 702 Silica Microspheres. Fishers, IN 2013, pp 3–4.

(30) Asylum Research. *MFP 3D SPM User Guide*, Version 13.; 2013.

(31) Darling, E. M.; Wilusz, R. E.; Bolognesi, M. P.; Zauscher, S.; Guilak, F. Spatial Mapping of the Biomechanical Properties of the Pericellular Matrix of Articular Cartilage Measured in Situ via Atomic Force Microscopy. *Biophys. J.* 2010, *98* (12), 2848–2856.

(32) Yoffe, E. H. Modified Hertz Theory for Spherical Indentation. *Philos. Mag. A Phys. Condens. Matter, Struct. Defects Mech. Prop.* 1984, *50* (6), 813–828.

(33) Poon, B.; Rittel, D.; Ravichandran, G. An Analysis of Nanoindentation in Linearly Elastic Solids. *Int. J. Solids Struct.* 2008, *45* (24), 6018–6033.

(34) Schulze, K. D.; Hart, S. M.; Marshall, S. L.; O'Bryan, C. S.; Urueña, J. M.; Pitenis, A. A.; Sawyer, W. G.; Angelini, T. E. Polymer Osmotic Pressure in Hydrogel Contact Mechanics. *Biotribology* 2017, *11*, 3–7.

(35) Valero, C.; Amaveda, H.; Mora, M.; García-Aznar, J. M. Combined Experimental and Computational Characterization of Crosslinked Collagen-Based Hydrogels. *PLoS One* 2018, *13* (4), 1–16.

(36) Chaudhuri, O. Viscoelastic Hydrogels for 3D Cell Culture. *Biomater. Sci.* 2017, *5* (8),

1480–1490.

(37) Chan, E. P.; Hu, Y.; Johnson, P. M.; Suo, Z.; Stafford, C. M. Spherical Indentation Testing of Poroelastic Relaxations in Thin Hydrogel Layers. *Soft Matter* **2012**, *8* (5), 1492–1498.

(38) Reale, E. R.; Dunn, A. C. Poroelasticity-Driven Lubrication in Hydrogel Interfaces. *Soft Matter* **2017**, *13* (2), 428–435.

(39) Delavoipière, J.; Tran, Y.; Verneuil, E.; Heurtefeu, B.; Hui, C. Y.; Chateauminois, A. Friction of Poroelastic Contacts with Thin Hydrogel Films. *Langmuir* **2018**, *34* (33), 9617–9626.

(40) Garcia, M.; Schulze, K. D.; O'Bryan, C. S.; Bhattacharjee, T.; Sawyer, W. G.; Angelini, T. E. Eliminating the Surface Location from Soft Matter Contact Mechanics Measurements. *Tribol. - Mater. Surfaces Interfaces* **2017**, *11* (4), 187–192.

(41) Rowe, K. G.; Dickrell, D. J.; Sawyer, W. G. Interrupted Measurement Repositioning Using Elastic Averaging. *Tribol. Lett.* **2015**, *59* (July), 0–3.

(42) Liu, H.; Bhushan, B. Adhesion and Friction Studies of Microelectromechanical Systems/Nanoelectromechanical Systems Materials Using a Novel Microtriboapparatus. *J. Vac. Sci. Technol. A Vacuum, Surfaces, Film.* **2003**, *21* (4), 1528–1538.

(43) Rennie, A. C.; Dickrell, P. L.; Sawyer, W. G. Friction Coefficient of Soft Contact Lenses: Measurements and Modeling. *Tribol. Lett.* **2005**, *18* (4).

(44) Sudre, G.; Hourdet, D.; Cousin, F.; Creton, C.; Tran, Y. Structure of Surfaces and Interfaces of Poly(N,N-Dimethylacrylamide) Hydrogels. *Langmuir* **2012**, *28* (33), 12282–12287.

(45) Tang, S.; Floy, M.; Bhandari, R.; Dziubla, T.; Hilt, J. Development of Novel N-Isopropylacrylamide (NIPAAm) Based Hydrogels with Varying Content of Chrysin Multiacrylate. *Gels* **2017**, *3* (4), 40.

(46) Dimitriadis, E. K.; Horkay, F.; Maresca, J.; Kachar, B.; Chadwick, R. S. Determination of Elastic Moduli of Thin Layers of Soft Material Using the Atomic Force Microscope. *Biophys. J.* **2002**, *82* (5), 2798–2810.

(47) Garabedian, N. T.; Khare, H. S.; Carpick, R. W.; Burris, D. L. AFM at the Macroscale: Methods to Fabricate and Calibrate Probes for Millinewton Force Measurements. *Tribol. Lett.* **2019**, *67* (1), 1–10.

(48) Lian, C.; Lin, Z.; Wang, T.; Sun, W.; Liu, X.; Tong, Z. Self-Reinforcement of PNIPAm-Laponite Nanocomposite Gels Investigated by Atom Force Microscopy Nanoindentation. *Macromolecules* **2012**, *45* (17), 7220–7227.

(49) Tanaka, Y.; Kawauchi, Y.; Kurokawa, T.; Furukawa, H.; Okajima, T.; Gong, J. P. Localized Yielding around Crack Tips of Double-Network Gels. *Macromol. Rapid Commun.* **2008**, *29* (18), 1514–1520.

(50) Liu, Y.; Lee, B. P. Recovery Property of Double-Network Hydrogel Containing a Mussel-Inspired Adhesive Moiety and Nano-Silicate. *J. Mater. Chem. B* **2016**, *4* (40), 6534–6540.

(51) Zhang, J.; Daubert, C. R.; Foegeding, E. A. Polyacrylamide Gels as Elastic Models for Food Gels: Fracture Properties Affected by Dextran and Glycerol. *J. Texture Stud.* **2006**, *37* (2), 200–220.

(52) Horkay, F.; Lin, D. C. Mapping the Local Osmotic Modulus of Polymer Gels. *Langmuir* **2009**, *25* (15), 8735–8741.

(53) Hutchings, I.; Shipway, P. *Tribology: Friction and Wear of Engineering Materials*, 2nd Editio.; Butterworth-Heinemann: London, 2017.

(54) Pitenis, A. A.; Urueña, J. M.; Schulze, K. D.; Nixon, R. M.; Dunn, A. C.; Krick, B. A.; Sawyer, W. G.; Angelini, T. E. Polymer Fluctuation Lubrication in Hydrogel Gemini Interfaces. *Soft Matter* **2014**, *10* (44), 8955–8962.

(55) Urueña, J. M.; Pitenis, A. A.; Nixon, R. M.; Schulze, K. D.; Angelini, T. E.; Gregory Sawyer, W. Mesh Size Control of Polymer Fluctuation Lubrication in Gemini Hydrogels. *Biotribology* **2015**, *1–2*, 24–29.

(56) Pitenis, A. A.; Urueña, J. M.; Cooper, A. C.; Angelini, T.; Sawyer, W. G. Superlubricity in Gemini Hydrogels. *J. Tribol.* **2016**, *138* (October), 7–9.

(57) Kim, J.; Dunn, A. C. Soft Hydrated Sliding Interfaces as Complex Fluids. *Soft Matter* **2016**, *12* (31).

(58) Pitenis, A. A.; Urueña, J. M.; Nixon, R. M.; Bhattacharjee, T.; Krick, B. A.; Dunn, A. C.; Angelini, T. E.; Sawyer, W. G. Lubricity from Entangled Polymer Networks on Hydrogels. *J. Tribol.* **2016**, *138* (4).

(59) Gaisinskaya, A.; Ma, L.; Silbert, G.; Sorkin, R.; Tairy, O.; Goldberg, R.; Kampf, N.; Klein, J. Hydration Lubrication: Exploring a New Paradigm. *Faraday Discuss.* **2012**, *156*, 217–233.

(60) Ma, L.; Gaisinskaya-Kipnis, A.; Kampf, N.; Klein, J. Origins of Hydration Lubrication. *Nat. Commun.* **2015**, *6*, 1–6.

(61) Klein, J.; Kumacheva, E.; Mahalu, D.; Perahla, D.; Fetterst, L. J. Reduction of Frictional Forces between Solid Surfaces Bearing Polymer Brushes. *Nature* **1994**, *370* (August), 634–636.

(62) Seror, J.; Zhu, L.; Goldberg, R.; Day, A. J.; Klein, J. Supramolecular Synergy in the Boundary Lubrication of Synovial Joints. *Nat. Commun.* **2015**, *6*, 1–7.

(63) Blanchet, T. A.; Kennedy, F. E. Sliding Wear Mechanism of Polytetrafluoroethylene (PTFE) and PTFE Composites. *Wear* **1992**, *153* (1), 229–243.

(64) Sun, J. Y.; Zhao, X.; Illeperuma, W. R. K.; Chaudhuri, O.; Oh, K. H.; Mooney, D. J.; Vlassak, J. J.; Suo, Z. Highly Stretchable and Tough Hydrogels. *Nature* **2012**, *489* (7414), 133–136.

(65) Haque, M. A.; Kurokawa, T.; Gong, J. P. Super Tough Double Network Hydrogels and Their Application as Biomaterials. *Polymer (Guildf).* **2012**, *53* (9), 1805–1822.
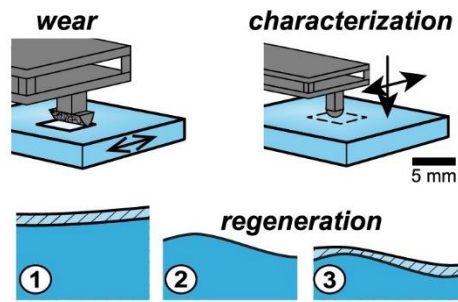
In this work, careful experiments reveal how abrasive wear of polyacrylamide hydrogels only temporarily alters the surface properties.